HHS Public Access

Author manuscript

*Nat Med*. Author manuscript; available in PMC 2013 July 01.

Published in final edited form as:

*Nat Med*. 2013 January ; 19(1): 74–82. doi:10.1038/nm.3040.

# Endothelial Apelin-FGF Link Mediated by MicroRNAs 424 and 503 is Disrupted in Pulmonary Arterial Hypertension

**Jongmin Kim**[1], **Yujung Kang**[1], **Yoko Kojima**[1], **Janet K. Lighthouse**[1], **Xiaoyue Hu**[1], **Micheala A. Aldred**[2], **Danielle L. McLean**[1], **Hyekyung Park**[1], **Suzy A. Comhair**[3], **Daniel M. Greif**[1], **Serpil C. Erzurum**[3], and **Hyung J. Chun**[1,†]

[1]Yale Cardiovascular Research Center, Section of Cardiovascular Medicine, Department of Internal Medicine, Yale University School of Medicine, New Haven, CT 06511

[2]Genomic Medicine Institute, The Lerner Institute, The Cleveland Clinic Foundation, Cleveland, OH 44195

[3]Department of Pathobiology, The Lerner Institute, The Cleveland Clinic Foundation, Cleveland, OH 44195

## Abstract

Pulmonary arterial hypertension is characterized by vascular remodeling associated with obliteration of pulmonary arterioles and formation of plexiform lesions comprised of hyperproliferative endothelial and vascular smooth muscle cells. Here, we describe a novel, microRNA-dependent association between APLN and FGF2 pathways in the pulmonary artery endothelial cells (PAECs), where disruption of APLN signaling results in a robust increase in FGF2 expression. We show that this link is mediated by two microRNAs, miR-424 and miR-503, that are regulated by APLN and significantly downregulated in PAH. MiR-424 and miR-503 exert anti-proliferative effects by targeting FGF2 and FGFR1. Overexpression of miR-424 and miR-503 in PAECs promoted cellular quiescence and inhibited the capacity of PAEC conditioned media to induce proliferation of pulmonary artery smooth muscle cells. We show that reconstitution of miR-424 and miR-503 can ameliorate pulmonary hypertension in experimental models. These studies demonstrate the importance of APLN-miR-424/503-FGF axis in maintaining pulmonary vascular homeostasis.

Pulmonary arterial hypertension (PAH) is a disease of the pulmonary vasculature that primarily targets the small pulmonary arteries. The hallmark of terminal PAH is plexiform



†to whom correspondences should be addressed: Hyung J. Chun, M.D., Yale University School of Medicine, Section of Cardiovascular Medicine, 300 George Street, Room 770H, New Haven, CT 06511, (203) 737-6389 (phone), (203) 737-6118 (fax), hyung.chun@yale.edu.

**Author Contributions**

J.K. and H.J.C. designed the research. J.K., Y.K., Y.K., J.K.L., X.H., D.L.M., H.P., and H.J.C. performed the experiments. M.A., S.A.C., and S.C.E. collected and prepared the subject samples, D.M.G. and S.C.E. assisted with data analysis and review of the manuscript. J.K. and H.J.C. prepared the figures. J.K and H.J.C. wrote the manuscript.

**Competing financial interests**

The authors declare no competing financial interests.

lesions comprised of hyperproliferative PAECs and pulmonary artery smooth muscle cells (PASMCs).[1] The abnormal proliferation of these cells likely involves perturbation of the inherent characteristics of both of these cell types, but emerging evidence suggest that pathologic crosstalk of dysregulated molecular signaling between these cells may also contribute to the disruption of the vascular homeostasis.[2–7]

Recent studies have described an emerging role for the APLN (also known as apelin)-APLNR (also known as apelin receptor, APJ and AGTRL1) signaling axis in the maintenance of pulmonary vascular homeostasis.[8,9] APLN is highly expressed in the endothelial cells of both the systemic and pulmonary vasculature.[10] The apelin receptor is thus far the only known receptor for APLN, and is also highly expressed in the lungs where it mediates the autocrine and paracrine effects of APLN in the pulmonary endothelium.[11,12] *Apln* knockout mice develop worsening pulmonary hypertension in response to hypoxia.[8] It has been found that APLN expression in serum and pulmonary endothelium of PAH subjects is significantly reduced.[8,9,13] The findings of hyperproliferative, anti-apoptotic phenotype of PAH PAECs, in conjunction with other studies demonstrating decreased APLN expression in PAH, suggest the possibility that disruption of APLN signaling in PAH PAECs results in the activation of a secondary signaling cascade that contributes to the aberrant proliferation of these cells.

Previous work from Folkman and colleagues demonstrated a significant increase in serum and urinary FGF2 levels in PAH subjects that may be important for disease pathogenesis.[14] A more recent study showed that the PAECs may be the primary source of increased FGF2 in PAH subjects.[5] Here we demonstrate the critical role of a novel, microRNA (miRNA)-based endothelial mechanism that integrates the reciprocal dysregulation of APLN and FGF2 signaling in PAH.

## Results

### Disruption of APLN signaling leads to increased FGF2 expression

Previous studies have demonstrated that APLN expression is significantly decreased in the serum and pulmonary microvascular endothelium of PAH subjects, as well as in the lungs of monocrotaline (MCT)-induced pulmonary hypertension.[8,9,13,15] In line with these data, we found that APLN expression is significantly decreased in multiple PAEC lines derived from lungs of idiopathic and familial PAH (IPAH and FPAH, respectively, referred as PAH from hereon) subjects compared to control PAECs from unused, explanted normal donor lungs (Fig. 1a–c). We found no significant difference in the mRNA levels of *APLNR*, which was predominantly expressed by the microvascular endothelial layers of the pulmonary vessels (Supp. Fig. 1a,b). We found increased PCNA (proliferating cellular nuclear antigen) staining in the endothelium of PAH microvasculature, as well as increased proliferative response of the PAH PAECs (Fig. 1c and Supp. Fig. 2). We also found that whereas augmentation of APLN signaling in normal PAECs led to an increase in PAEC proliferation as previously described,[9] augmentation of APLN signaling in PAH PAECs had a reverse effect of inhibiting proliferation (Supp. Fig. 3).

Given these findings, we hypothesized that downregulation of APLN in PAH PAECs may be contributing to the aberrant activation of a secondary signaling cascade leading to increased proliferation of PAECs. We evaluated the expression of an array of angiogenic growth factors in PAECs subjected to *APLN* knockdown (Supp. Fig. 4) and found that FGF2 expression was significantly increased (Fig. 1d). We also found a strong, inverse correlation between *APLN* and *FGF2* mRNA levels in the PAECs from control and PAH subjects (Fig. 1e). We confirmed this relationship by demonstrating a robust increase in FGF2 expression with *APLN* knockdown, and reciprocally decreased FGF2 levels with *APLN* overexpression (Fig. 1f). To further explore the relationship between APLN and FGF2, we examined FGF2 levels in *Apln* null mice and found significantly increased expression of FGF2 in the total lung homogenates and isolated mouse lung endothelial cells (LECs) (Fig. 1g).[16]

## FGF2 is regulated by miRNAs downstream of APLN signaling

We hypothesized that APLN regulation of FGF2 may be secondary to a novel miRNA mediated mechanism that affects the stability of the *FGF2* mRNA. To test this hypothesis, we first determined whether knockdown of *AGO2* (Argonaute2), a key catalytic core component of the RNA-induced silencing complex, can lead to increased FGF2 expression in PAECs. We found that knockdown of *AGO2* (Supp. Fig. 4) indeed led to a robust increase in FGF2 protein level in normal PAECs, suggesting the presence of a basal miRNA-directed FGF2 regulation in PAECs (Fig. 1h). Moreover, the higher FGF2 expression in the PAECs of a PAH subject was not affected by *AGO2* knockdown, suggesting that the miRNA-mediated mechanism of FGF2 regulation may be compromised in these PAECs (Fig. 1h). In addition, we found that the reduced FGF2 expression seen with *APLN* overexpression was abrogated by concurrent *AGO2* knockdown (Fig. 1i).

Based on these findings, we conducted a miRNA microarray analysis to identify miRNAs regulated by APLN that may be involved in FGF2 regulation. We conducted microarray analyses using PAECs subjected to knockdown of 1) *APLN*, 2) *APLNR*, and 3) *APLN* + *APLNR* (Fig. 2a and Supp. Fig. 5). From a total of 14 miRNAs that were significantly downregulated in each of the three conditions (Supp. Table 1), *in silico* analysis (www.microRNA.org) identified two that were predicted to target the *FGF2* 3′ untranslated region (UTR): miR-424 and miR-503, which are separated by 250 basepairs on the X chromosome and share a significant homology in their respective seed sequences (Fig. 2b). None of the other miRNAs that were significantly decreased targeted *FGF2*. Moreover, miRNAs predicted to target *FGF2*, including miR-15a, miR-16, miR-195 and miR-497, were not significantly changed in the array experiments (data not shown). We confirmed via real-time quantitative PCR that both the pri-form and the mature form of miR-424 and miR-503 are significantly downregulated with *APLN* knockdown (Fig. 2c), suggesting that the transcription of these miRNAs, rather than their post-transcriptional maturation, appears to be regulated by APLN signaling. We also found that these two miRNAs are transcribed as a single transcript which is also APLN regulated (Supp. Fig. 6a,b). We generated a putative miR-424/503 promoter based luciferase reporter construct, which was robustly induced by *APLN* overexpression in PAECs (Fig. 2d). Moreover, we found decreased mmu-miR-322 (hsa-miR-424 homolog in mouse) and miR-503 levels in both the total lung homogenates and LECs from *Apln* null mice (Fig. 2e). We found that the lungs had high expression of

miR-424 and miR-503, similar to what has been described for *APLN* (Fig. 2f).[17] *In situ* hybridization of human lungs demonstrated robust expression of miR-424 and miR-503 in the pulmonary vascular luminal layer of the pulmonary microvasculature (Fig. 2g and Supp. Fig. 7).

To validate the predicted targeting of FGF2 by miR-424 and miR-503, we determined the effects of miR-424 and miR-503 overexpression or knockdown on FGF2 expression in PAECs. Remarkably, miR-424 and miR-503 were predicted to target the *FGF2* 3′ UTR at three separate sites (Supp. Fig. 8). We found that FGF2 expression was significantly decreased with miR-424 or miR-503 overexpression in normal and PAH PAECs, while transfection of anti-miRs that inhibit endogenous miRNA function in normal PAECs led to a reciprocal increase of FGF2 expression (Fig. 3a and Supp. Fig. 9a,b). Furthermore, we generated luciferase constructs with the 3′ UTR sequence of the *FGF2* gene and found a robust decrease of luciferase activity in response to miR-424 and miR-503 overexpression (Fig. 3b). This response was abrogated when we mutated the miR-424 and miR-503 targeted seed sequences (Fig. 3b).

## MiR-424 and miR-503 target FGFR1 and are regulators of FGF signaling

We further analyzed the *in silico* data to identify additional putative targets of miR-424 and miR-503 that may play a role in FGF signaling. We found that *FGFR1*, a key receptor in the FGF signaling pathway, was also predicted to be targeted by miR-424 (as recently described[18]) and miR-503, as it has two distinct miR-424 and miR-503 binding sites in its 3′ UTR (Supp. Fig. 8). We found that overexpression or knockdown of miR-424 and miR-503 in normal and PAH PAECs targeted FGFR1 expression in a similar manner as FGF2 (Fig. 3a and Supp. Fig. 9a,b), and the luciferase reporter bearing the 3′ UTR of *FGFR1* was also similarly affected by miR-424 and miR-503 overexpression (Fig. 3b). Mutation of the miR-424 and miR-503 targeted seed sequences in the *FGFR1* 3′ UTR led to complete abrogation of miR-424- and miR-503-mediated inhibition of luciferase reporter activity (Fig. 3b). Lastly, we found that *APLN* knockdown resulted in robust increases of FGF2 and FGFR1, that were abrogated with concurrent overexpression of miR-424 and miR-503 (Fig. 3c).

We next determined whether the perturbation of miR-424 and miR-503 can affect phosphorylation of ERK1/2, a key downstream target of FGF2/FGFR1 signaling in endothelial cells.[19] We found that baseline ERK1/2 phosphorylation was decreased with miR-424 and miR-503 overexpression both at basal state and with exogenous FGF2 stimulation, likely secondary to reduction of FGFR1 expression (Fig. 3d). In addition, we found that transfection of anti-miRs against miR-424 and miR-503 led to a significant increase in ERK1/2 phosphorylation (Fig. 3e).

## MiR-424 and miR-503 downregulation correlates with FGF2 and FGFR1 upregulation in PAH PAECs

Given that *APLN* expression is significantly decreased in PAH PAECs, our findings would suggest that miR-424 and miR-503 expression would also be reduced in these cells. Indeed, we found significantly decreased expression of the mature, pri, and pre forms of miR-424

and miR-503 in PAECs derived from PAH subjects (Fig. 4a and Supp. Fig. 10a,b). Moreover, we found significantly increased *FGF2* mRNA levels in the PAH PAECs (Fig. 4a).

There was a significant linear correlation between the mRNA levels of *APLN* and miR-424 as well as miR-424 and miR-503, and a significant inverse correlation between miR-424/503 and *FGF2/FGFR1* mRNA levels (Fig. 4b and Supp. Fig. 11). We found markedly higher FGF2 and FGFR1 protein expression by western blots in all of the PAH PAEC lysates evaluated (Fig. 4c). In addition, immunohistochemistry against FGFR1 in the lung samples of unused explanted donor and PAH subject showed significantly higher expression of FGFR1 in the endothelial layer of the PAH lung, as demonstrated by co-localization with von Willebrand Factor (VWF) (Fig. 4d). *In situ* hybridization of lungs from PAH subjects demonstrated significantly lower levels of miR-424 and miR-503 in the microvasculature compared to control donor lungs (Fig. 4e and Supp. Fig. 12).

## MiR-424 and miR-503 promote PAEC quiescence

We conducted a series of experiments using human PAECs to further evaluate the functional role of miR-424 and miR-503. We found that the endogenous expression levels of miR-424 and miR-503 increased as the PAECs reached a confluent state, or in serum-starvation conditions (Supp. Fig. 13). Cell cycle analysis showed that overexpressing miR-424 and miR-503 induced G0/G1 cell cycle arrest in both normal PAECs and in PAH PAECs (Fig. 5a). Overexpression of miR-424 and miR-503 using miRNA mimics led to a significantly decreased proliferation of normal and PAH PAECs, whereas *FGFR1* transfection (lacking the 3′ UTR) in conjunction with FGF2 stimulation reversed the inhibition of proliferation with miR-424 and miR-503 overexpression in normal and PAH PAECs (Fig. 5b and Supp. Fig. 14). Moreover, the increased proliferation of normal PAECs in response to *APLN* overexpression was further augmented with concurrent inhibition of miR-424 and miR-503, and inhibition of miR-424 and miR-503 reversed the anti-proliferative effect of *APLN* overexpression on PAH PAECs (Supp. Fig. 3b).

We found that transfection of siRNAs against *FGF2* and *FGFR1* (Supp. Fig. 4) led to a significantly reduced PAH PAEC proliferation (Supp. Fig. 14). Inhibition of miR-424 or miR-503 led to a significantly increased proliferation of normal PAECs but had minimal effect on PAH PAECs (Fig. 5c). In addition, concurrent knockdown of *FGF2* and *FGFR1* completely antagonized the effects of miR-424 and miR-503 inhibition on control PAECs, while inhibiting proliferation of PAH PAECs (Fig. 5c). PAEC migration was also reduced by overexpression of miR-424 and miR-503 in control and PAH PAECs (Fig. 5d,e), which was reversed by restoration of FGF2 and FGFR1 in control PAECs (Fig. 5d).

## Paracrine inhibition of PASMC proliferation by endothelial miR-424 and miR-503

As PAH is a vascular disease that is characterized by hyperproliferation of both PAECs and PASMCs, we tested whether there was any significant change in miR-424 and miR-503 expression in PAH PASMCs. We found that PASMCs had significantly lower transcript levels of miR-424 and miR-503 than PAECs, and we saw no significant change in miR-424 or miR-503 expression in PAH PASMCs compared to control PASMCs (Supp. Fig. 15a,b).

We next evaluated whether overexpression of miR-424 and miR-503 in PAECs can affect the proliferation of PASMCs in a paracrine manner. We found that incubation of PASMCs with conditioned media (CM) from control PAECs resulted in a significant increase in PASMCs proliferation, whereas CM from PAH PAECs induced a greater degree of PASMC proliferation (Fig. 5f). When the PASMCs were incubated with CM from either control or PAH PAECs transfected with miR-424 and miR-503, the proliferative response of the PASMCs was significantly reduced. Moreover, we found that the miR-424/503 effect was abrogated by concurrently transfecting PAECs with an *FGF2* overexpression construct, demonstrating the ability of FGF2 to reverse the PAEC derived paracrine effects of miR-424 and miR-503 (Fig. 5f). In further validating the APLN-miR-424/503-FGF2/FGFR1 link, we found that CM from normal PAECs subjected to *APLN* knockdown induced a significant increase in PASMC proliferation, which was reduced to baseline by concurrent overexpression of miR-424/503 in PAECs (Fig. 5g). Knockdown of *FGF2* in PAECs also led to decreased proliferation of PASMCs subjected to PAEC CM (Fig. 5h). Moreover, the hyperproliferative response of PASMCs to CM from PAEC subjected to *APLN* knockdown was abrogated by concurrent knockdown of *FGF2* (Fig. 5h).

### MiR-424 and miR-503 ameliorate experimental pulmonary hypertension

We evaluated the expression levels of rno-miR-322 (hsa-miR-424 homolog in rat), miR-503, FGF2, and FGFR1 in two experimental models of pulmonary hypertension in rats: the MCT model and the SU-5416/hypoxia (SuHx) model.[20,21] We found that rats subjected to MCT or SuHx had significantly decreased expression of miR-322 and miR-503 in the lungs and isolated LECs, decreased *Apln* expression in the LECs, as well as a robust increase in FGF2 and FGFR1 expression (Fig. 6a,b,g). We validated the miR-322(424)/503-FGF2/FGFR1 axis in rats by demonstrating that FGF2 and FGFR1 expression in isolated rat LECs are significantly downregulated by overexpressing rno-miR-322 or rno-miR-503 mimics (Supp. Fig. 16), or human miR-424 or miR-503 (data not shown). We evaluated the efficacy of miR-424 and miR-503 restoration in ameliorating the severity of pulmonary hypertension in three separate models: 1) MCT prevention model, 2) MCT rescue model, and 3) SuHx rescue model (Supp. Fig. 17). We used intranasal delivery of either control lentivirus with GFP (GFP) or lentivirus containing miR-424 and miR-503 (424/503-GFP, $2\times10^{10}$ pfu per intranasal delivery) to induce expression of these miRNAs in the lungs ($n$ = 6–9 in each group). We confirmed the expression of the lentiviral miRNAs by detecting the lentiviral specific miR-424 and miR-503 transcripts in the lung homogenates as well as isolated LECs of 424/503-GFP treated rats, which was absent in the GFP group (Supp. Fig. 18a). Expression was also confirmed by detection of lentivirally-expressed copGFP in both the 424/503-GFP and GFP treated rat lungs, but not in control rat lungs (Supp. Fig. 18b). Confirmation of endothelial infection was determined by flow cytometry, with identification of $CD31^+$, $GFP^+$ population (~8% of $CD31^+$ cells) in the lentiviral groups (Supp. Fig. 18c). Lastly, we found restoration of miR-424 (rno-miR-322 and lentivirally-expressed hsa-miR-424) and miR-503 levels in the isolated LECs of SuHx-424/503-GFP group that was comparable to the non-diseased control state (Supp. Fig. 18d).

As expected, all three models tested demonstrated a significant increase in the right ventricular systolic pressures (RVSP) (Fig. 6c). Remarkably, we found marked reduction of

RVSP in the rats that received intranasal 424/503-GFP compared to those that received GFP (Fig. 6c). We also found a significant reduction in the right ventricle to left ventricle + septum (RV/LV+S) weight ratio in the 424/503-GFP groups (Supp. Fig. 19). The number of muscularized microvessels was also significantly lower in the 424/503-GFP groups in each of the three models (Fig. 6d). To evaluate for any change in vascular proliferation, we performed PCNA staining in conjunction with vWF staining. We found increased number of PCNA-positive microvessels in the pulmonary hypertension rats in the GFP control groups, whereas those in the 424/503-GFP groups had significantly fewer PCNA positive microvessels (Fig. 6e). We also found in the SuHx model increased number of obliterated vessels in the GFP group, which was significantly reduced in the 424/503-GFP group (Fig. 6f). Lastly, there was significantly decreased FGF2 and FGFR1 expression in the total lungs as well as isolated LECs of the 424/503-GFP groups, further validating the miR-424/503-FGF2/FGFR1 axis (Fig. 6g).

## Discussion

Recent studies have associated decreased APLN expression with clinical PAH.[8,9,13] In addition, abnormal elevation of FGF2 has also been linked with PAH.[5,14] Here we describe a novel, miRNA-driven regulation of FGF signaling by APLN that integrates these isolated clinical observations into a cohesive mechanism that provides greater insights into the perturbations of the signaling paradigms that occur in PAH.

The importance of APLN signaling in the pulmonary vascular homeostasis is beginning to emerge, as demonstrated by the exacerbation of hypoxia-induced pulmonary hypertension in *Apln* null mice, and reversal of disease upon exogenous apelin peptide administration in the MCT model and in the endothelial specific PPARγ knockout mice.[8,9,15] Our findings provide four major conclusions: 1) FGF2 expression in PAECs is robustly increased by disruption of APLN signaling, 2) miR-424 and miR-503 are key miRNAs that are intricately regulated by APLN and target two key components of endothelial FGF signaling—FGF2 and FGFR1, 3) downregulation of APLN, miR-424 and miR-503 in PAH PAECs is associated with robust increase in FGF2 and FGFR1 expression and hyperproliferation of PAECs and PASMCs, and 4) restoration of miR-424 and miR-503 in the lungs inhibits FGF2 and FGFR1 expression and ameliorates experimental models of pulmonary hypertension.

The downstream targets of APLN in the context of the pulmonary vasculature remain to be fully elucidated. Our current findings demonstrate that APLN signaling, in a miR-424 and miR-503 dependent manner, serves a critical role in regulating the magnitude of FGF signaling in the pulmonary vasculature (Fig. 6h). Although basal FGF signaling activity has been found to be essential for endothelial homeostasis,[19] it has also been shown that the pathological augmentation of FGF signaling is associated with the cellular hyperproliferation and vascular remodeling found in PAH.[5,14,22] These findings indicate that the maintenance of a delicately balanced FGF signaling is essential for the preservation of pulmonary vascular homeostasis. Previous studies have suggested proliferative effects of APLN on endothelial cells. Nevertheless, these effects have been modest at best, and others have refuted such findings,[23] suggesting a strong context-dependence for APLN's effects on

the endothelium. APLN appears to have the greatest proliferative and migratory effects in the developing vasculature,[24–26] but these findings have not been convincingly extended to the mature endothelium. Rather, an emerging role of APLN signaling in mature vessels appears to be to preserve a differentiated, quiescent, and homeostatic endothelial layer. This role is mediated at least in part by induction of KLF2 and NOS3 (eNOS) expression,[8] and the enhancement of endothelial layer integrity via maintenance of membranous CDH5 (VE-Cadherin) expression.[27] Our current data point to a third role, where miR-424 and miR-503 are induced by APLN to serve as crucial rheostats to inhibit aberrant cellular growth and proliferation. It is worth noting that in addition to the cellular growth inhibitory effects described here of the APLN-miR-424/miR-503 axis, APLN signaling can also promote cellular growth via other signaling targets, as previously described.[9] Nevertheless, our demonstration of marked reduction of APLN, miR-424 and miR-503 expression and its sequelae in PAH PAECs shed light on the importance of this signaling axis in maintenance of pulmonary vascular homeostasis.

Prior work demonstrated that increased production of FGF2 from the PAECs may play an important role in the pathogenesis of PAH.[5,14,22] However, the mechanism of this dysregulation has remained undefined. Our study is the first demonstration of an intrinsic, miRNA-mediated regulation of FGF signaling that is essential to maintain homeostasis in the pulmonary vasculature. Our data also provide a mechanism by which restoration of miR-424 and miR-503 expression in PAECs can regulate PASMC growth in a paracrine manner. These findings lend further support for the emerging role of PAEC-PASMC crosstalk that likely plays an important role in the pathogenesis of PAH.[5–7]

Although no prior studies have demonstrated a role for miR-424 or miR-503 in PAH, miR-322(424) was found to be significantly downregulated in array analyses evaluating the MCT model of pulmonary hypertension in rats.[28] Studies have also implicated miR-424 and miR-503 in promoting the differentiation of monocytes, macrophages and skeletal muscle.[29,30] A recent study demonstrated targeting of VEGF, VEGFR2 and FGFR1 by miR-424 in HUVECs, but a separate study indicated that miR-424 may have a pro-angiogenic function in hypoxic endothelial cells, suggesting a possible context-dependent role for miR-424.[18,31] Further investigation to define the mechanism of APLN-mediated regulation of miR-424 and miR-503 are ongoing and will provide greater insights into the mechanism regulating endothelial expression and function of these critical miRNAs.

Although we cannot completely rule out the possibility that other validated targets of miR-424 and miR-503 such as CCNE1, cdc25A, MEK1, VEGF, and VEGFR2 may also contribute to the PAEC phenotype of PAH subjects, we found no significant changes in their expression levels in PAH PAECs (unpublished data). Furthermore, we found that restoration or abrogation of FGF signaling was sufficient to fully counter the effects of either overexpression or knockdown of miR-424 and miR-503 in PAECs, respectively. It is possible that additional predicted but not yet validated targets of miR-424 and miR-503 may also contribute to the cellular and *in vivo* consequences of modulating these miRNAs. Given that the current study focused on the regulatory mechanism that links APLN signaling to the FGF2 signaling cascade in the pulmonary vasculature, future studies will be needed to

evaluate the role of other validated and predicted targets of miR-424 and miR-503 in the context of PAH.

In summary, we have defined a novel relationship between the APLN and FGF signaling pathways in the pulmonary vasculature that is mediated by two APLN-responsive miRNAs: miR-424 and miR-503. We have shown that downregulation of these miRNAs is associated with both human PAH as well as established experimental rodent models. These findings support development of novel therapeutic strategies targeting augmentation of APLN and miR-424/miR-503 signaling, as well as inhibition of FGF signaling.

## Online Methods

### Human samples

We obtained human lung tissues were obtained from either unused, explanted donor lungs or explanted lungs from confirmed subjects with PAH undergoing lung transplantation at the Cleveland Clinic. Additional PAH and normal donor lung samples were obtained from the National Disease Research Interchange. The study was approved by the Cleveland Clinic and the Yale University School of Medicine Institutional Review Boards.

### Animal studies

Animal experiments performed in this study were approved by the Institutional Animal Care and Use Committee of Yale University. *Apln* knockout mice have been described previously.[8,16]

### Cell culture and reagents

We isolated PAECs from normal and PAH explanted donor lungs, as described previously.[32,33] We obtained additional control PAECs from Lonza. PAECs from 10 controls and 13 IPAH or FPAH (10 IPAH and 3 FPAH) subjects were studied. In brief, human pulmonary arteries were dissected from the lungs to the distal small arterioles, and PAECs were harvested from the isolated pulmonary arterial tree. PAECs were grown in EBM-2 basal media supplemented with EGM-2 (Lonza) on fibronectin coated plates. Cells were passaged at 70–80% confluency, and primary cultures of passages 3–7 were used in experiments. PASMCs from control donors and PAH subjects were isolated as previously described.[33,34] In brief, elastic pulmonary arteries were dissected from lungs obtained at explantation during lung transplant. After removal of endothelial cells, PASMCs were dissociated with collagenase type II/DNase I and cells were cultured in SMC growth medium (Lonza). Primary cultures of passages 5–7 were used in experiments. We used HeLa cells (ATCC) for the 3′ UTR targeting luciferase assays. Human Angiogenesis Antibody Array (R&D Systems) was used with PAEC lysates from cells transfected with either control siRNA or *APLN* siRNA. Recombinant human FGF2 was used at 20 ng $mL^{-1}$ (R&D Systems). Apelin-13 peptide was used at 1 μM (Sigma).

### Antibodies

Antibodies to FGF2 (Cat. # 610072, 1:1000 dilution, BD Biosciences), FGFR1 (Cat. # 3472s, 1:1000 dilution, Cell Signaling), GAPDH (Cat. # 2118s, 1:1000 dilution, Cell

Signaling), phospho-ERK1/2 (Cat. # 4377, 1:1000 dilution, Cell Signaling), ERK1/2 (Cat. # 9102, 1:1000 dilution, Cell Signaling), APLN (Cat. # SC-33469, 1:200 dilution, Santa Cruz), and cop-GFP (Cat. # AB513, 1:20,000 dilution, Evrogen) were used for western blotting. Antibodies to von Willebrand Factor (Cat. # A0082, 1:200 dilution, DAKO), PCNA (proliferating cellular nuclear antigen) (Cat. # M0879, 1:200 dilution, DAKO), SMA (smooth muscle actin)-Cy3 (Cat. # C6198, 1:250 dilution, Sigma), APLN (Cat. # SC-33469, 1:200 dilution, Santa Cruz) and FGFR1 (Cat. # AB10646, 1:200 dilution, ABCAM) were used for immunofluorescence. Mouse antibody to rat-CD31 (Clone # TLD-3A12, 1:100 dilution, BD Biosciences) and Alexa Fluor 647 Goat antibody to mouse IgG (Cat. # A-21236, 1:200 dilution, Invitrogen) were used for flow cytometry.

### SiRNAs, microRNA mimics and anti-miRs

Short interfering RNAs (siRNAs) against *APLN*, *AGO2*, *FGF2*, and *FGFR1*, as well as non-targeting controls were purchased from Invitrogen. Ambion miR-424 (Cat. # PM10306), miR-503 (Cat. # PM10378), anti-miR-424 (Cat. # AM10306) and anti-miR-503 (Cat. # AM10378) were used for *in vitro* transfections. SiRNA, miRNA mimics and anti-miRs were complexed with Lipofectamine RNAiMAX (Invitrogen) according to the manufacturer's instructions. Control miRNA (Cat. # AM17110), or control anti-miRNA (Cat. # AM17010) (Ambion) were used for negative controls.

### RNA extraction, reverse transcription PCR and miRNA profiling

We extracted total RNA with the miRNeasy RNA isolation kit (Qiagen). Purified RNA was reverse transcribed with iScript™ cDNA Synthesis Kit (Bio-Rad). RT-PCR was performed with TaqMan probes for both genes and miRNAs (Applied Biosystems). RT-PCR for miR-424 detected both the human (hsa-miR-424) and rodent (rno-miR-322 and mmu-miR-322) variants. All miRNA data were normalized to the internal control small RNAs *RNU19* and *HY3* for human samples and *U87* for rat samples. For the mRNA samples, ribosomal 18S was used as an internal control. Individual RT-PCRs were performed on a CFX96 (Bio-Rad) according to the manufacturer's instructions.

### MicroRNA array

We used the Illumina microRNA expression profiling panel (based on miRbase release 9.0) for miRNA analysis according to the manufacturer's recommendation (Illumina, Inc., San Diego, CA). Human PAECs (Lonza) subjected to 1) control, 2) *APLN*, 3) *APLNR*, or 4) *APLN* + *APLNR* siRNA transfection. Each experimental condition was performed in triplicate. RNA samples (200 ng) from each condition were first labeled and then hybridized to each array using standard Illumina protocols. Sample array matrices were scanned on an Illumina BeadArray reader. Data were imported into GenomeStudio (Illumina), quantile-normalized and log2-transformed in R (www.r-project.org).

### Immunohistochemistry of lung sections

Small pieces of fixed human and rat lung tissue were rehydrated through an ethanol series to 1xPBS and cryo-protected in 30% sucrose (in 1xPBS) at 4 °C overnight. Tissue was then embedded in OCT (Sakura Tissue-Tek), frozen solid in cryomolds, sectioned on a Leica

CM1950 at 10 μm and stored at −20 °C. Cryosections were then air-dried for 10 min at room temperature, and rehydrated in 1xPBS for 15 min at room temperature. Sections were treated with 5% $H_2O_2$ (in 1xPBS) for 30 min at room temperature to reduce auto fluorescence from elastic lamina and red blood cells. Sections were washed in 1xPBS, blocked in 5% heat-inactivated goat serum in 1xPBS for 1 h at room temperature, and then probed with primary antibody overnight at 4 °C. After incubation, slides were washed with 1xPBS, blocked for 1 h at room temperature, and probed with Alexa 488 goat antibody to rabbit and DAPI at 10 ug $mL^{-1}$ overnight at 4 °C. After washing, slides were mounted in mounting media (DAKO) and sealed with nail polish. Hematoxylin and eosin staining was performed using standard methods.

### *In situ* hybridization

Paraffin embedded human lung tissues were deparaffinized and rehydrated through an ethanol series. Slides were washed in PBS containing 3% $H_2O_2$ for 30 min to quench endogenous peroxidase activity. After proteinase K digestion for 5 min, slides were fixed in 4% paraformaldehyde and rinsed in PBS. Slides were incubated in hybridization buffer for 2 hr at 60 °C. Probes for miR-424, miR-503, or scrambled miR control (50 nM, DIG labeled LNA probes, Exiqon) were mixed with hybridization buffer, heated to 90 °C for 4 min, chilled on ice and added to the sections, followed by incubation overnight at 60 °C and stringent washes in wash buffer (50% formamide in 2X SSC and PBST). We generated the *APLNR* probe from full length *APLNR* cDNA (Thermo Scientific) cloned into pCMV-Sport6 vector. Digoxigenin (DIG)-labeled riboprobe was prepared from the recombinant plasmid using a DIG RNA Labeling Kit (SP6/T7) from Roche Applied Science (Germany). Incubation was done at 65 °C overnight. For alkaline phosphatase (AP) reaction, AP substrate (NBT/BCIP-Roche-11681451001) was used and the slides were mounted in aqueous mounting medium. For immunofluorescent imaging, DIG was detected by a digoxigenin-specific, horseradish peroxidase–labeled antibody (Roche-11207733910) and amplified with a TSA-Plus Cy3 system (Perkin Elmer-NEL744). This was followed by staining with vWF as described in immunohistochemistry method.

### Oligonucleotide primers

All primers were obtained from the Keck Oligonucleotide Synthesis Resource at Yale University (Supp. Table 2).

### Isolation of mouse and rat lung endothelial cells

We isolated mouse and rat lung endothelial cells (LECs) by digesting whole lung tissue with collagenase (2mg $mL^{-1}$) with gentle agitation for 45 min at 37 °C. Using a 30 mL syringe attached firmly to a cannula, suspension was triturated 12 times, the cell suspension was filtered through 70 μm cell strainers, and centrifuged at 400 g for five min at 4 °C. Cells were resuspended in 2 mL of cold PBS + 0.1% BSA and the cell suspension was incubation with Dynabeads with sheep antibody to mouse IgG (Invitrogen) coated with purified antibody to CD31 (BD Pharmingen). We performed second sorting to ensure the purity of the LECs.

### Vectors, plasmids and luciferase assays

Human *FGF2* 3′-UTR (874 bp) and *FGFR1* 3′-UTR (1906 bp) that included the predicted miR-424/503 seed sequences were amplified using from a human genomic DNA by PCR and confirmed by sequencing. The *FGF2* 3′-UTR and *FGFR1* 3′-UTR were cloned into the XhoI and NotI sites of psiCHECK-2 (Promega). CTGCT in the three predicted seed sequences of *FGF2* and two predicted seed sequences of *FGFR1* (Supp. Fig. 8) were mutated to TAATA. We transfected HeLa cells with the luciferase reporter constructs containing the 3′ UTR variants and with 30 nM of either miR-424/503 mimics or negative control miRNA using Lipofectamine 2000 (Invitrogen). The cells were lysed and luciferase activity was measured 24 h post-transfection by Dual Luciferase Assay System (Promega). The *FGFR1* and *FGF2* expression constructs lacking the 3′ UTR were used (Addgene and Origene). Putative human miR-424/503 promoter sequence was amplified using primers from human genomic DNA by PCR and confirmed by sequencing. The PCR product was cloned into the KpnI and HindIII sites of PGL3 vector (Promega) using In-Fusion® PCR Cloning System (Clontech). PAECs were transfected with miR-424/503 promoter-luciferase, renilla-luciferase, and *APLN* constructs (Origene). At 24h post-transfection, luciferase activity was quantified using the Dual-Luciferase Reporter Assay kit (Promega).

### Protein methods

We performed western blotting as previously described.[8,35] Each western blot is a representative of three independent experiments done in triplicates. For generation of cell lysates, RIPA lysis buffer (Thermo Scientific) containing Halt Protease and Phosphatase Inhibitor cocktail (Thermo Scientific) was used. Protein contents were measured using a Bio-Rad DC assay kit.

### Northern blots for microRNAs

For Northern blot analysis, total RNA (10μg) was resolved on a 15% denaturing polyacrylamide gel and transferred to Hybond N+ nylon membrane (Amersham). The membranes were crosslinked using stratagene UV crosslinker and prehybridization were performed at 58 °C in DIG Easy Hyb (Roche). Probes for miR-424 and miR-503 (DIG labeled LNA probes, Exiqon) were mixed with DIG Easy Hyb and incubated overnight at 58 °C and were washed with 2xSSC, 0.1% SDS for 15 min at 50 °C and then with 0.5xSSC, 0.1%SDS for an additional 15 min at 50 °C. The blot was blocked with 5% milk powder in PBST for 30 min at RT and incubated with anti-DIG-AP (Roche) in blocking buffer for 1 h at room temperature. After washing, detection was performed with CDP-star chemiluminescent substrate (Roche).

### Proliferation Assays

PAECs ($5\times10^3$ cells well$^{-1}$) were plated to a 96-well plate and transfected with miRNA or anti-miRNAs with Lipofectamine RNAiMax (Invitrogen). PAEC proliferation was assessed under basal condition (2% FCS). For the MTT assay, cell proliferation was measured by the CellTiter 96® AQueous One Solution Cell Proliferation Assay kit (Promega). To assess PASMC proliferation, PASMCs were seeded at $2\times10^4$ cells per well in a 24-well plate. The cells were allowed to adhere for 24 h then washed three times and starved in serum free

media for 48h. These quiescent cells were then stimulated with conditioned media and proliferation measured using the MTT assay.

To assess dynamic cell proliferation, we used the xCELLigence system (Roche), which monitors cell growth in response to APLN treatment in real-time. PAECs were seeded at 2,000 cells per well in 96 well E-Plates. The cells were monitored every 30 min for the indicated period.

### Cell cycle analysis and flow cytometry

PAECs transfected with miRNA mimics or anti-miRs were fixed in ethanol, treated with RNase A and subsequently stained with propidium iodide (PI). DNA content was analyzed by flow cytometry (BD FACScan). Data quantification was performed using FlowJo 7.6. Flow cytometry for CD31 and GFP was performed using BD FACScan and data analyzed using FlowJo 7.6.

### Cell migration assay

PAEC migration was analyzed using a 24-well cell-migration assay (Radius Assay, Cell Biolabs, Inc.) per manufacturer's protocol. Migration images were captured with microscope and migration closure was measured using Image J software.

### Lentivirus production

Lenti-miR microRNA precursors for hsa-miR-424 and hsa-miR-503 were used along with GFP control lentivirus (System Biosciences). For *APLN* overexpression in PAECs, full length human *APLN* cDNA (Origene) was cloned into CD511B-1 lentiviral vector (System Biosciences). The Lenti-X HTX Packaging System (Clontech) with Lenti-X Concentrator was used to generate the lentivirus particles for intranasal delivery and *in vitro* cellular transduction.

### Monocrotaline and SU-5416/hypoxia induction of pulmonary hypertension and intranasal administration of lentivirus

Male Sprague Dawley rats (200–250 g) were subcutaneously injected with monocrotaline (60 mg $kg^{-1}$) (Sigma). For the SU-5416/hypoxia model, we resuspended SU-5416 (20 mg $kg^{-1}$) (Sigma) in DMSO and injected subcutaneously. Rats were subsequently exposed to hypoxia (10% $FiO_2$) for three weeks. Intranasal administration of either the lenti-GFP or lenti-424/503-GFP ($2\times10^{10}$ pfu per intranasal delivery per rat) was performed at the designated times (Supp. Fig. 17). We anesthetized rats with inhaled isoflurane and subsequently placed lentiviral droplets (~250 μL) over their nares for inhalation.

### Hemodynamic and morphometric analysis

RVSP measurements were performed at the designated time point after pulmonary hypertension induction in rats under isoflurane anesthesia by inserting a catheter (Millar Instruments) via the right jugular vein as described previously.[8] Lungs were perfused with normal saline, and fixed in 4% paraformaldehyde overnight for immunohistochemistry, or snap frozen in liquid nitrogen for protein and RNA analyses. The hearts were dissected and

weighed for calculation of the RV hypertrophy index (RV/[LV + S]). The same full section in the mid-portion of the left lung parallel to the hilum was used and embedded in the same manner for morphometric analyses. Pulmonary artery muscularization was assessed at 200x magnification after staining for SMA by calculating the ratio of fully and partially muscularized peripheral pulmonary arteries to total peripheral pulmonary arteries in 5 random fields per lung (1 field = 200x magnification). The total number of vessels less than 75 μm was expressed as the number of vessels counted per random microscope field (5 random fields per lung at 200x magnification). All measurements were carried out by investigators blinded to the experimental condition. The number of obliterated vessels was counted in 5 random fields per lung and averaged among the rats in each group.

### Statistical analysis

All experiments were performed in triplicate (unless otherwise specified) from at least three independent experiments, and data shown are means ± S.E.M. When only 2 groups were compared, statistical differences were assessed with unpaired 2-tailed Student's *t* test. Otherwise statistical significance was determined using 1-way ANOVA followed by Bonferroni multiple comparison test. Relationships between variables were determined by the Pearson correlation coefficient. A *P* value less than 0.05 was considered statistically significant.

## Supplementary Material

Refer to Web version on PubMed Central for supplementary material.

## Acknowledgments

We thank M. Simons and P. Yu for critical reading of the manuscript, R. Homer for pathology slide review, T. Quertermous (Stanford University) for the *Apln* null mice, and P. Lee and Y. Zhang for guidance with the lentiviral work. This study was supported by grants from the US National Institutes of Health (HL095654, HL113005 and HL101284 to H.J.C., HL069170 to S.C.E. and HL093362 to D.M.G.), Howard Hughes Medical Institute (Physician Scientist Early Career Award to H.J.C.), American Heart Association Grant-in-Aid (12GRNT9410029 to H.J.C.) and Pfizer ASPIRE Young Investigator Research Award (H.J.C.).

## References cited

1. Tuder RM, Marecki JC, Richter A, Fijalkowska I, Flores S. Pathology of pulmonary hypertension. Clin Chest Med. 2007; 28:23–42. vii. [PubMed: 17338926]
2. Humbert M, et al. Cellular and molecular pathobiology of pulmonary arterial hypertension. J Am Coll Cardiol. 2004; 43:13S–24S. [PubMed: 15194174]
3. Hassoun PM, et al. Inflammation, growth factors, and pulmonary vascular remodeling. J Am Coll Cardiol. 2009; 54:S10–19. [PubMed: 19555853]
4. Schermuly RT, Ghofrani HA, Wilkins MR, Grimminger F. Mechanisms of disease: pulmonary arterial hypertension. Nature reviews Cardiology. 2011; 8:443–455. [PubMed: 21691314]
5. Izikki M, et al. Endothelial-derived FGF2 contributes to the progression of pulmonary hypertension in humans and rodents. J Clin Invest. 2009; 119:512–523. [PubMed: 19197140]
6. Eddahibi S, et al. Cross talk between endothelial and smooth muscle cells in pulmonary hypertension: critical role for serotonin-induced smooth muscle hyperplasia. Circulation. 2006; 113:1857–1864. [PubMed: 16606791]
7. Dewachter L, et al. Angiopoietin/Tie2 pathway influences smooth muscle hyperplasia in idiopathic pulmonary hypertension. Am J Respir Crit Care Med. 2006; 174:1025–1033. [PubMed: 16917117]

8. Chandra SM, et al. Disruption of the apelin-APJ system worsens hypoxia-induced pulmonary hypertension. Arterioscler Thromb Vasc Biol. 2011; 31:814–820. [PubMed: 21233449]
9. Alastalo TP, et al. Disruption of PPARgamma/beta-catenin-mediated regulation of apelin impairs BMP-induced mouse and human pulmonary arterial EC survival. J Clin Invest. 2011; 121:3735–3746. [PubMed: 21821917]
10. Sheikh AY, et al. In vivo genetic profiling and cellular localization of apelin reveals a hypoxia-sensitive, endothelial-centered pathway activated in ischemic heart failure. Am J Physiol Heart Circ Physiol. 2008; 294:H88–98. [PubMed: 17906101]
11. Hosoya M, et al. Molecular and functional characteristics of APJ. Tissue distribution of mRNA and interaction with the endogenous ligand apelin. J Biol Chem. 2000; 275:21061–21067. [PubMed: 10777510]
12. Regard JB, Sato IT, Coughlin SR. Anatomical profiling of G protein-coupled receptor expression. Cell. 2008; 135:561–571. [PubMed: 18984166]
13. Goetze JP, et al. Apelin: a new plasma marker of cardiopulmonary disease. Regul Pept. 2006; 133:134–138. [PubMed: 16263185]
14. Benisty JI, et al. Elevated basic fibroblast growth factor levels in patients with pulmonary arterial hypertension. Chest. 2004; 126:1255–1261. [PubMed: 15486390]
15. Falcao-Pires I, et al. Apelin decreases myocardial injury and improves right ventricular function in monocrotaline-induced pulmonary hypertension. Am J Physiol Heart Circ Physiol. 2009; 296:H2007–2014. [PubMed: 19346461]
16. Charo DN, et al. Endogenous regulation of cardiovascular function by apelin-APJ. Am J Physiol Heart Circ Physiol. 2009; 297:H1904–1913. [PubMed: 19767528]
17. Habata Y, et al. Apelin, the natural ligand of the orphan receptor APJ, is abundantly secreted in the colostrum. Biochim Biophys Acta. 1999; 1452:25–35. [PubMed: 10525157]
18. Chamorro-Jorganes A, et al. MicroRNA-16 and MicroRNA-424 Regulate Cell-Autonomous Angiogenic Functions in Endothelial Cells via Targeting Vascular Endothelial Growth Factor Receptor-2 and Fibroblast Growth Factor Receptor-1. Arterioscler Thromb Vasc Biol. 2011; 31:2595–2606. [PubMed: 21885851]
19. Murakami M, et al. The FGF system has a key role in regulating vascular integrity. J Clin Invest. 2008; 118:3355–3366. [PubMed: 18776942]
20. Stenmark KR, Meyrick B, Galie N, Mooi WJ, McMurtry IF. Animal models of pulmonary arterial hypertension: the hope for etiological discovery and pharmacological cure. Am J Physiol Lung Cell Mol Physiol. 2009; 297:L1013–1032. [PubMed: 19748998]
21. Taraseviciene-Stewart L, et al. Inhibition of the VEGF receptor 2 combined with chronic hypoxia causes cell death-dependent pulmonary endothelial cell proliferation and severe pulmonary hypertension. FASEB J. 2001; 15:427–438. [PubMed: 11156958]
22. Tu L, et al. Autocrine fibroblast growth factor-2 signaling contributes to altered endothelial phenotype in pulmonary hypertension. Am J Respir Cell Mol Biol. 2011; 45:311–322. [PubMed: 21037114]
23. Kalin RE, et al. Paracrine and autocrine mechanisms of apelin signaling govern embryonic and tumor angiogenesis. Dev Biol. 2007; 305:599–614. [PubMed: 17412318]
24. del Toro R, et al. Identification and functional analysis of endothelial tip cell-enriched genes. Blood. 2010; 116:4025–4033. [PubMed: 20705756]
25. Kasai A, et al. Apelin is a crucial factor for hypoxia-induced retinal angiogenesis. Arterioscler Thromb Vasc Biol. 2010; 30:2182–2187. [PubMed: 20705920]
26. Kasai A, et al. Retardation of retinal vascular development in apelin-deficient mice. Arterioscler Thromb Vasc Biol. 2008; 28:1717–1722. [PubMed: 18599802]
27. Kidoya H, Naito H, Takakura N. Apelin induces enlarged and nonleaky blood vessels for functional recovery from ischemia. Blood. 2010; 115:3166–3174. [PubMed: 20185589]
28. Caruso P, et al. Dynamic changes in lung microRNA profiles during the development of pulmonary hypertension due to chronic hypoxia and monocrotaline. Arterioscler Thromb Vasc Biol. 2010; 30:716–723. [PubMed: 20110569]

29. Forrest AR, et al. Induction of microRNAs, mir-155, mir-222, mir-424 and mir-503, promotes monocytic differentiation through combinatorial regulation. Leukemia. 2010; 24:460–466. [PubMed: 19956200]
30. Sarkar S, Dey BK, Dutta A. MiR-322/424 and -503 are induced during muscle differentiation and promote cell cycle quiescence and differentiation by down-regulation of Cdc25A. Mol Biol Cell. 2010; 21:2138–2149. [PubMed: 20462953]
31. Ghosh G, et al. Hypoxia-induced microRNA-424 expression in human endothelial cells regulates HIF-alpha isoforms and promotes angiogenesis. J Clin Invest. 2010; 120:4141–4154. [PubMed: 20972335]
32. Masri FA, et al. Hyperproliferative apoptosis-resistant endothelial cells in idiopathic pulmonary arterial hypertension. Am J Physiol Lung Cell Mol Physiol. 2007; 293:L548–554. [PubMed: 17526595]
33. Comhair SA, et al. Human primary lung endothelial cells in culture. Am J Respir Cell Mol Biol. 2012; 46:723–730. [PubMed: 22427538]
34. Aytekin M, et al. High levels of hyaluronan in idiopathic pulmonary arterial hypertension. Am J Physiol Lung Cell Mol Physiol. 2008; 295:L789–799. [PubMed: 18776053]
35. Chun HJ, et al. Apelin signaling antagonizes Ang II effects in mouse models of atherosclerosis. J Clin Invest. 2008; 118:3343–3354. [PubMed: 18769630]

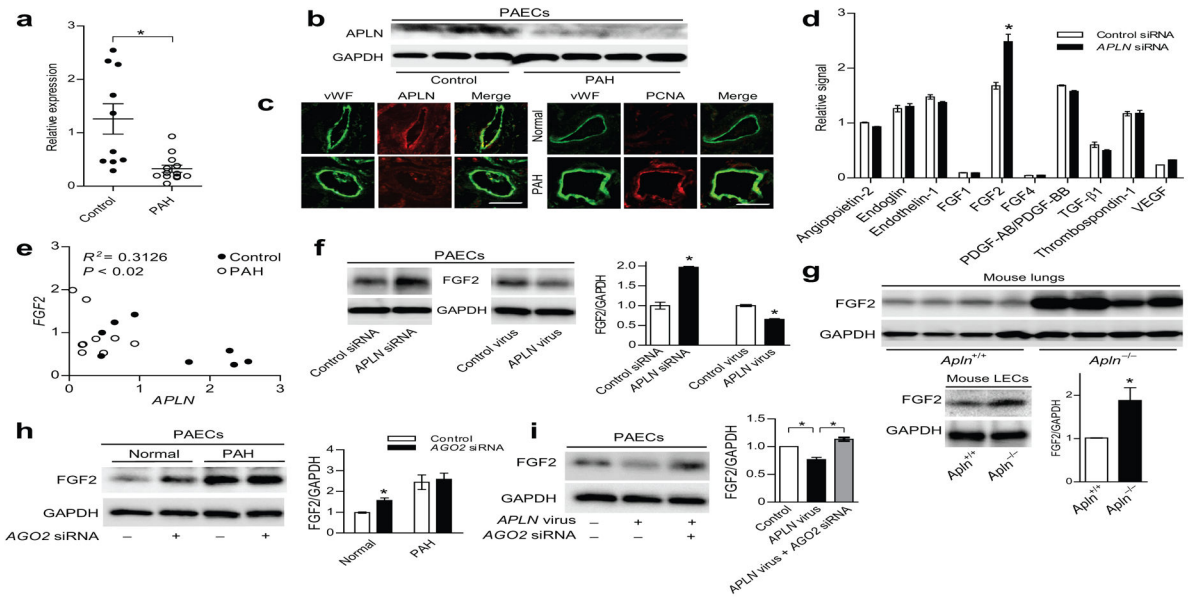


**Figure 1. APLN reciprocally regulates FGF2 expression in PAECs in a miRNA dependent manner**

(**a**) *APLN* mRNA expression in PAECs of controls and PAH subjects. **P* < 0.005 vs. controls. (**b**) APLN protein expression in PAECs of controls and PAH subjects. (**c**) Immunofluorescence staining showing APLN expression and PCNA staining in the lung endothelium of a control and a PAH subject. Von Willebrand Factor (vWF) staining is shown in green, APLN and PCNA staining are shown in red. Scale bar = 50 μm. (**d**) Cytokine array showing relative changes in cytokine expression in response to *APLN* knockdown in PAECs. **P* < 0.01 vs. control siRNA. (**e**) Correlation between *APLN* and *FGF2* mRNA levels in PAECs from normal controls and PAH subjects. (**f**) Expression of FGF2 protein in response to either *APLN* knockdown or lentiviral *APLN* overexpression in PAECs. **P* < 0.01. (**g**) Expression of FGF2 protein in total lung homogenates and isolated LECs from wildtype and *Apln* null mice. **P* < 0.05. (**h**) FGF2 expression in response to knockdown of *AGO2* in normal and PAH PAECs. **P* < 0.01. (**i**) FGF2 expression in PAECs in response to *APLN* overexpression and *AGO2* knockdown. **P* < 0.01.

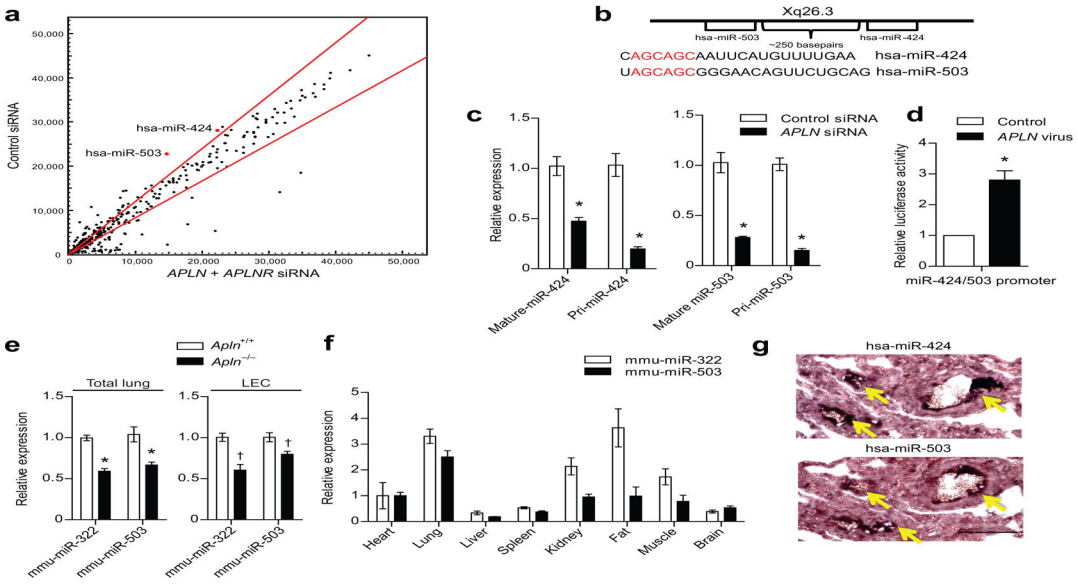


**Figure 2. APLN-FGF2 reciprocal axis is mediated by APLN regulated expression of miR-424 and miR-503**

(**a**) MiRNA microarray analysis of PAECs subjected to *APLN* and *APLNR* knockdown. MiR-424 and miR-503 are depicted in red. Red lines demarcate a 1.2 fold change from baseline expression. (**b**) Chromosomal location of miR-424 and miR-503 and the sequences of the mature miRNAs. The homology in the seed sequences is depicted in red. (**c**) Quantitative PCR showing expression of the mature and pri-forms of miR-424 and miR-503 in response to *APLN* knockdown in PAECs. **P* < 0.01 vs. control siRNA. (**d**) Relative luciferase activity of PAECs transfected with the putative miR-424 and miR-503 promoter based luciferase reporter construct in response to *APLN* overexpression. **P* < 0.001. (**e**) Expression of mmu-miR-322 (mouse homolog of hsa-miR-424) and mmu-miR-503 expression in total lungs and LECs of *Apln* deficient mice. **P* < 0.001 and †*P* < 0.01. (**f**) Quantitative PCR of mmu-miR-322 and mmu-miR-503 of mouse tissues. (**g**) *In situ* hybridization of human lungs for miR-424 and miR-503. Yellow arrows depict positive staining cells. Scale bar = 100 μm.

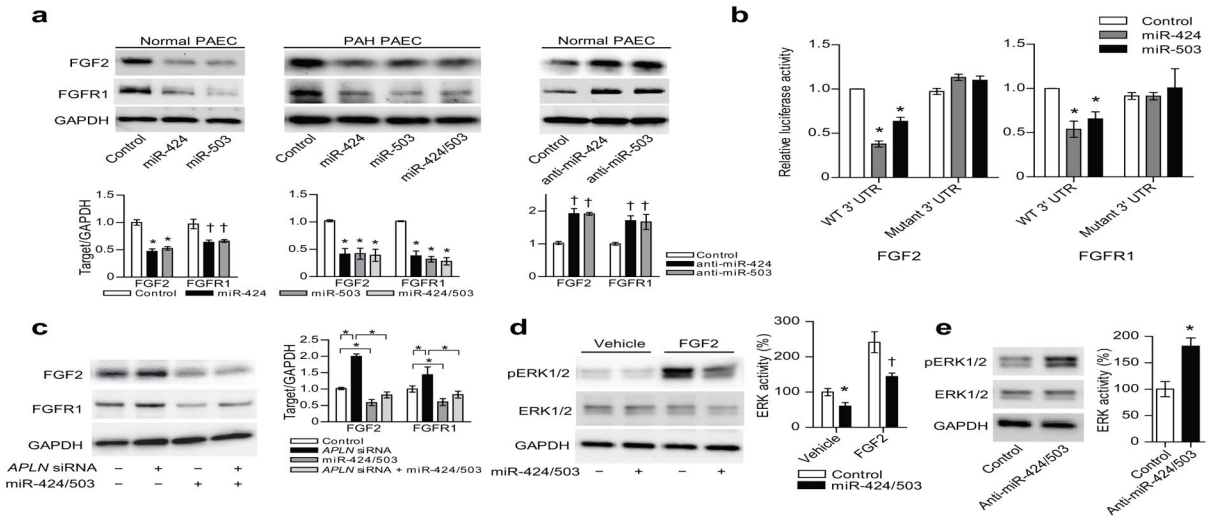


**Figure 3. MiR-424 and miR-503 regulate FGF2 and FGFR1 expression and signaling**

(**a**) FGF2 and FGFR1 protein expression in response to either overexpression of miR-424 and miR-503 in normal and PAH PAECs, and inhibition of miR-424 or miR-503 in normal PAECs. **P* < 0.01 and †*P* < 0.05. (**b**) Targeting of *FGF2* and *FGFR1* 3′ UTR by miR-424 and miR-503. Both wildtype (WT) and mutagenized 3′ UTR constructs are shown. **P* < 0.01 vs. control. (**c**) FGF2 and FGFR1 expression in response to knockdown of *APLN* in PAECs with concurrent overexpression of miR-424 and miR-503. **P* < 0.01. (**d**) ERK1/2 phosphorylation in response to overexpression of miR-424 and miR-503 in PAECs, both at baseline and with FGF2 stimulation. **P* < 0.05 and †*P* < 0.01. (**e**) ERK1/2 phosphorylation with inhibition of miR-424 and miR-503 with anti-miRs in PAECs. **P* < 0.01.

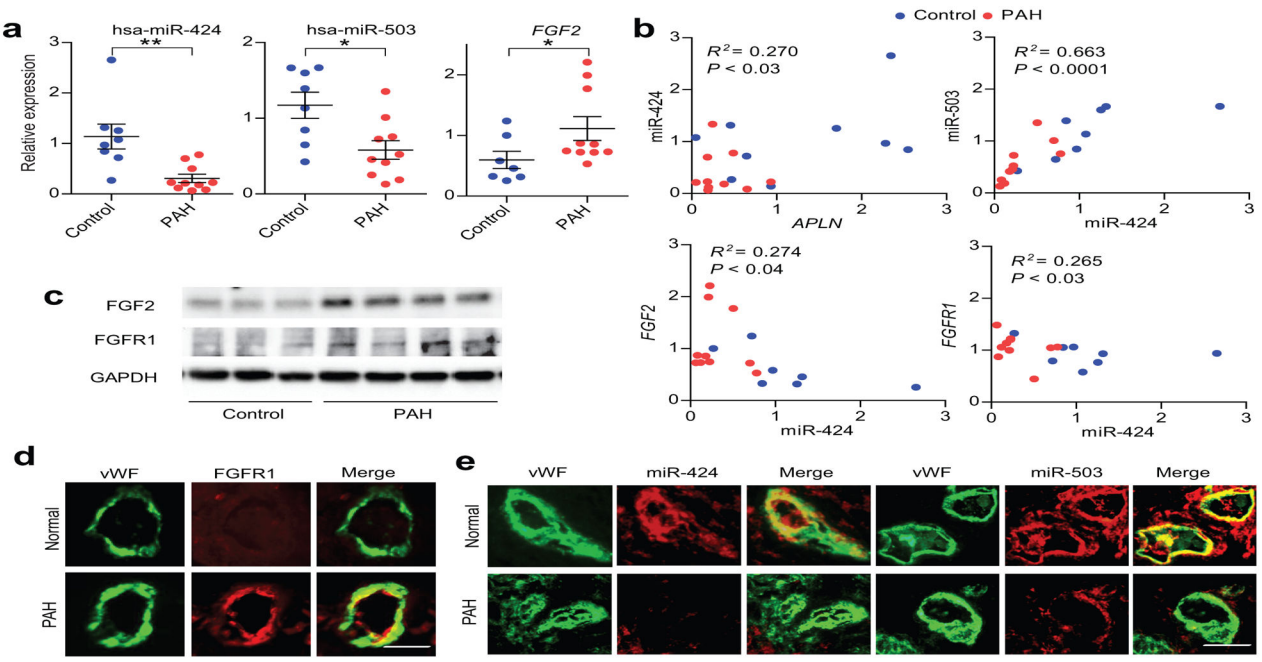


**Figure 4. Downregulation of miR-424 and miR-503 in PAH is associated with increased FGF2 and FGFR1 expression**

(**a**) Expression of miR-424, miR-503, and *FGF2* mRNA in PAECs of controls and PAH subjects. **P* < 0.01, ***P* < 0.05. (**b**) Correlation plots for expression levels of *APLN* mRNA and miR-424, miR-424 and miR-503, *FGF2* mRNA and miR-424, and *FGFR1* mRNA and miR-424 in PAECs from control and PAH PAECs. (**c**) Expression of FGF2 and FGFR1 proteins in control and PAH PAECs. (**d**) FGFR1 expression (shown in red) in control and PAH lung microvascular endothelium with costaining for vWF (shown in green). (**e**) Expression of miR-424 and miR-503 by *in situ* hybridization (shown in red) in the pulmonary endothelium (vWF staining in green) in the microvasculature of control and PAH lungs. Scale bar = 50 μm.

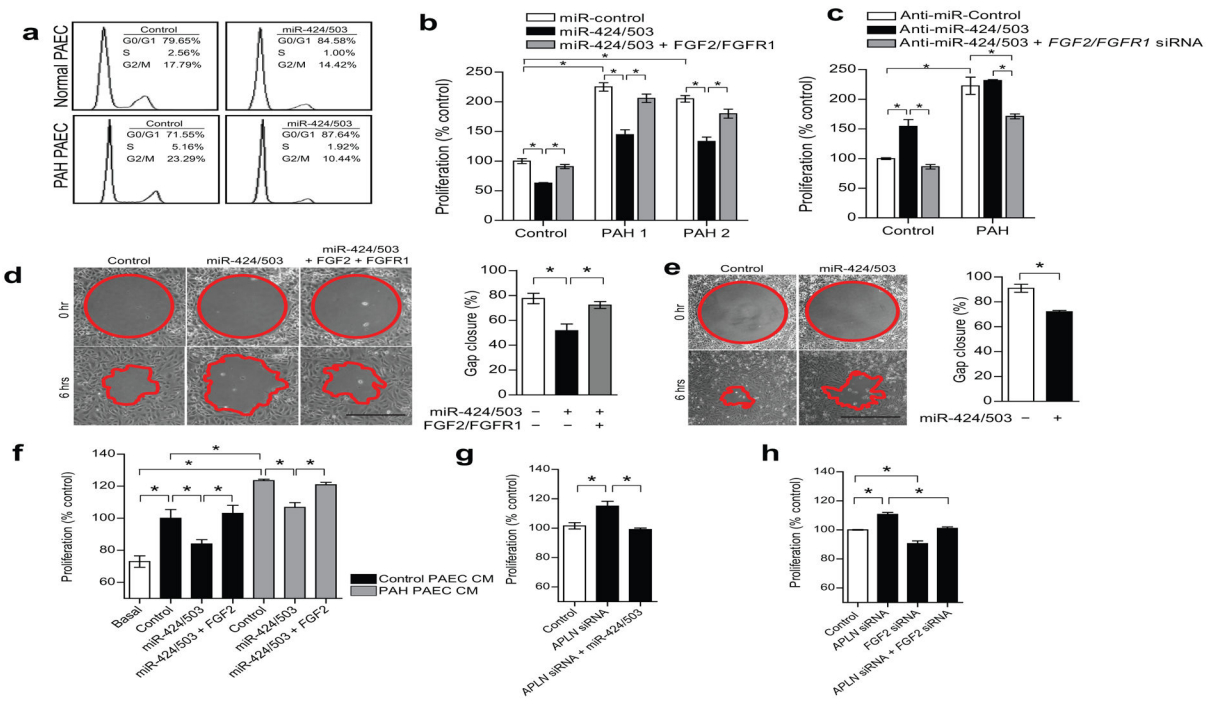


**Figure 5. Endothelial miR-424 and miR-503 regulate PAEC proliferation and migration and induce paracrine inhibition of PASMC proliferation**

(a) Cell cycle analysis of PAECs with miR-424 and miR-503 overexpression in normal and PAH PAECs. (b) Proliferation of normal and PAH PAECs with overexpression of miR-424 and miR-503 or with concurrent stimulation with exogenous FGF2 and transfection of *FGFR1* expression construct. **P* < 0.01. (c) Proliferation of normal PAECs and PAH PAECs in response to inhibition of miR-424 and miR-503 by anti-miR transfection or with concurrent knockdown of *FGF2* and *FGFR1*. **P* < 0.01. (d) Cell migration response to miR-424 and miR-503 overexpression or with concurrent FGF2 stimulation and *FGFR1* trasfection in normal PAECs. **P* < 0.05 vs. controls. Scale bar = 500 μm. (e) Cell migration response to overexpression of miR-424 and miR-503 in PAH PAECs. **P* < 0.05. Scale bar = 500 μm. (f) PASMC proliferation in response to conditioned media (CM) from PAECs of a normal donor and a PAH subject (Control vs. Basal), CM from respective PAECs transfected with miR-424 and miR-503 mimics, and co-transfected with *FGF2* expression construct. **P* < 0.01. (g) PASMC proliferation in response to CM from PAECs subjected to either *APLN* knockdown alone or in conjunction with miR-424 and miR-503 overexpression. **P* < 0.05. (h) Proliferation of PASMCs in response to CM from PAECs subjected to APLN knockdown, FGF2 knockdown, or concurrent knockdown. **P* < 0.05.

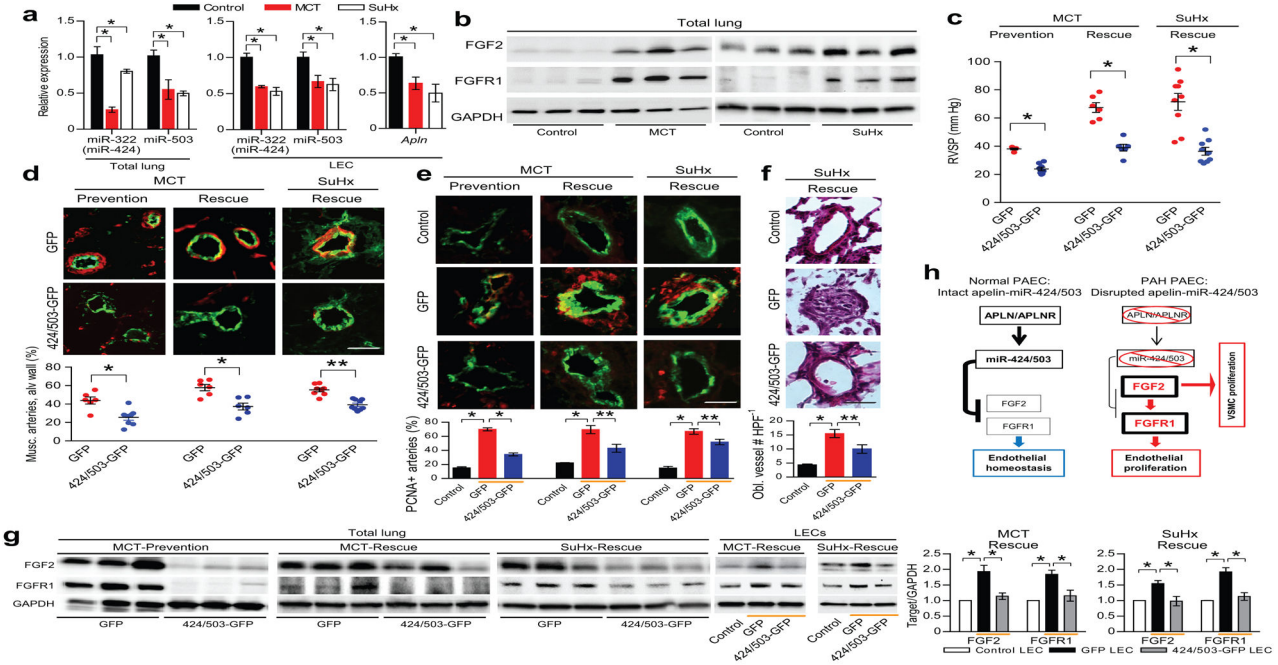

**Figure 6. MiR-424 and miR-503 can ameliorate the experimental pulmonary hypertension models in rodents**

(**a**) Expression levels of rno-miR-322 (hsa-miR-424 equivalent in rat) and miR-503 in rat lungs and isolated LECs 3 weeks after MCT injection and 4 weeks after SuHx. Expression levels of *Apln* mRNA in the rat LECs from two pulmonary hypertension models. *$P < 0.01$. (**b**) Expression of FGF2 and FGFR1 in the MCT and SuHx induced pulmonary hypertension rat lungs. (**c**) Right ventricular systolic pressure (RVSP) measurements in rats receiving intranasal delivery of lentiviral miR-424 and miR-503 (424/503-GFP) compared to control lentivirus (GFP) in the MCT prevention and rescue models, and the SuHx rescue model. *$P < 0.001$ for each model. (**d**) Microvascular muscularization analysis of lungs from rats receiving either intranasal GFP or 424/503-GFP in the three models. Smooth muscle actin is shown in red, vWF is shown in green. *$P < 0.01$ and **$P < 0.001$. (**e**) Assessment of PCNA expression in the lungs of the three pulmonary hypertension models receiving either GFP control or 424/503-GFP. PCNA is shown in red, vWF is shown in green. Orange bars denote the experimental pulmonary hypertension groups. *$P < 0.001$ and **$P < 0.01$. (**f**) H&E staining of the lungs from rats subjected to SuHx pulmonary hypertension induction receiving either GFP or 424/503-GFP. The average number of obliterated vessels per microscopic field is shown. Orange bars denote the experimental pulmonary hypertension groups. *$P < 0.001$, **$P < 0.02$. (**g**) FGF2 and FGFR1 protein levels in the lung homogenates of rats in the three models with either GFP or 424/503-GFP. FGF2 and FGFR1 expression in the isolated LECs from the MCT-Rescue and SuHx-Rescue models with GFP or 424/503-GFP. Orange bars denote the experimental pulmonary hypertension groups. *$P < 0.05$. (**h**) Proposed mechanism of endothelial signal linking APLN, miR-424/miR-503, and FGF2-FGFR1 in normal and PAH pulmonary endothelium.